SPRING COLLEGE ON PLASMA PHYSICS

15 May - 9 June 1989

OPTICAL DIAGNOSTICS FOR PLASMA-FOCUS DEVICE

R. Miklaszewski

Institute of Plasma Physics & Laser Microfusion
Warsaw
Poland

OPTICAL DIAGNOSTICS FOR PLASMA-FOCUS DEVICE

R.MIKLASZEWSKI
Institute of Plasma Physics and
Laser Microfusion
Warsaw, POLAND

1. INTRODUCTION

One of the most useful diagnostic methods for plasma investiga-
tions uses an electromagnetic wave propagating across the plasma as a
source of informations about plasma parameters. These methods are gene-
rally referred as "optical methods" and they include:

- optical interferometry which enables to measure the plasma
  density,

- Schlieren and shadowgraphy which give information on the first
  and second drivatives of the plasma density,

- Faraday rotation methods based on the measurement of the rota-
  tion of the polarization plane of the wave crossing the plasma
  which enables to measure distribution of the magnetic field in
  plasma,

- scattering methods giving density, temperature and turbulence
  structure.

The first and the second of these methods are very well establis-
hed in several areas of investigations especially in areodynamics, for
more than half century. Actually the optical methods of interferometry
and Shlieren and shadowgraph photography are widely used in laboratory
plasmas whose configuration can be reasonably assumed to have one or
two-dimensional symmetry.

The progress in high-brightness light sources particulary the
invention and developement of lasers orginated a rapid growth of inte-
rest in these methods. The monochromaticity, collimation, high brightness
and short duration of the laser pulse have greatly simplified the inhe-
rent difficulties of the standard interferometric set-ups. Additionally
feasible measurements of the Faraday rotation became feasible in the
optical region after the discovery of the laser sources.

Great efforts are being made in the developement of the scattering
methods as they could be helpful in understanding of the microscopic
behaviour of the plasma. Although the discovery of the lasers made such
measurement conceivable on laboratory plasmas, the requirements on the
power, monochromaticity of the light and precision of detecting and
analysing of a very low scattered signals are so serious that the met-
hod is very difficult in application. Nevertheless there are numerous
examples of successful utilization of scattering methods in plasma inves-
tigations 1), 2) etc.

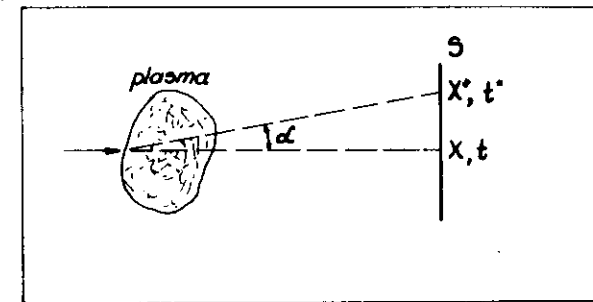Let us consider an electromagnetic wave propagating across a plas-
ma (Fig.1).

Fig.1. Propagation of a light ray through a density inhomogenity.

An individual ray which in the absence of any disturbance would
reach the screen S at the point X at the time t, if there is a plasma
on its way it would reach the screen at point X^* at time t^*. The inser-
tation of appropriate optical equipment into the light path will furnish
on S a record of the following:

-) the phase lag $\tau = t^* - t$
-) the deflection α
-) the displacement $d = x^* - x$

If an electromagnetic wave is initially polarized and the plasma
is magnetized with nonzero component of B field parallel to they ray
direction, the rotation of the polarization plane will occur.

An interferometer is a device which is able to record time lag,
a schlieren is that which records deflections, a shadowgraph records
displeacements and a polarimeter measures changes of the polarization
plane of the wave.

2. PLASMA REFRACTIVITY

The effects of the phase lag and a ray deflection are manifestation of changes of the refractivity index. The index of refraction n is defined as:

$$n = \frac{c}{V_p} = \frac{c\,k\,(\omega)}{\omega}$$

V_p - phase velocity
k - wave number (1)

Although the term "plasma" describes a fully ionized gas of zero net charge density, in general one deals with gaseous mixture of: free electrons, residual neutral atoms, atoms once, twice ... or campletly ionized etc. The refractivity of the gaseous mixture (here including neutral and charged particles) can be considered as the sum of the refractivities of the various components. Therefore we can write, for the refractivity of the plasma.

$$n = 1 + \sum_i K_i\,N_i$$

where N_j is the density of the i-th component of the mixture and K_i is the specific refractivity.

The problem of plasma and wave interaction has been wide investigated. The most complete description of wave phenomena is obtained by solving the Boltzman transport equations and the complete set of Maxwell equations. Detailed description of this problem and various froms of dispersion relations can be found in basic plasma handbooks and review papers 3), 4).

In the most simple case of fully ionized plasma, neglecting the ion plasma frequency which is much lower than the electron one the expression for the refractive index can be approximated as:

$$n^2 = 1 - \frac{\omega_{pe}}{\omega^2}$$ ω_{pe} - electron plasma frequency (2)

This formula shows that the propagation of an electromagnetic wave is possible only if $\omega > \omega_{pe}$.

To pervent intense absorbtion, reflection and deflection the wave frequency should be much greater then the plasma one. Thus the condition the electromagnetic wave length should fulfil can be written as:

$$\lambda^2 \ll \frac{1 \cdot 12 \cdot 10^{22}}{N_e}$$ $N_e\ [cm^{-3}]$
$\lambda\ [\mu m]$ (3)

For $\omega \gg \omega_{pe}$ the expression of the refractive index (2) can be approximated to the first order by:

$$n \cong 1 - \frac{1}{2} \cdot \frac{\omega^2_{pe}}{\omega^2}$$ (4)

This is the formula commonly used in practice.

In the case of a magnetized plasma the problem is more complicated and the formula for the refractive idex depends on the value of a magnetic field, plasma density and the angle between a magnetic field and wave number.
The various effects of an external magnetic field are practically negligible if $\omega \gg \Omega_e$ (Ω_e - electron gyro-frequency) that is if 3):

$$B \ll \frac{1.07 \cdot 10^2}{\lambda}\ [MGs]\ ,\ \lambda\,[\mu m]$$ (5)

In the case of noncomplet ionization, the refractive index is influenced by the presence of neutral atoms. The refractivity of the neutral gas can be approximated by Cauchy's formula of the from:

$$n = 1 + A + \frac{B}{\lambda^2}$$ (6)

where the values of the coefficients A and B can be found in 5) for several gases.
The condition for the refractive effect of the residual neutral atoms neglection is 3):

$$\frac{N_e}{N} \gg 0.83 \cdot 10^3 \frac{A}{\lambda^2}$$ (7)

A - first coefficient of the Cauchy formula
Ne, N - electron and neutral atoms density $[cm^{-3}]$

It should be noticed that the refractive index of neutral atoms is greater than unity and has an inverse squere dependence on

In case that all previous inequalities are satisfied, the refractivity of the plasma can be expressed by formula (4). However, we wish to emphasize the fact that a careful inquiry into the actual existing experimental conditions **is required each time one uses approximation (4) 3).**

3. INTERFEROMETRY

Interferometry is conceptually the most direct technique for mea-
surements exploiting plasma refractivity. It leads directly to a density
determination by comparing the optical path length trough a plasma with
the equivalent optical path length in the absence of the plasma.

Two different approaches to the interferometric density measure-
ments are possible:

- spatial coverage (line-of-sight integrated) at one instant in
  time - used for plasma-focus and z-pinch investigations (pulse
  lasers in visible range),

- temporal coverage integrated along one line of sight

  - applied for instance in tokamaks (CW - lasers in submilimeter
    range).

Although the theoretical basis of the two approuches is the same,
but they are realized in different ways. The following text is limited
to the former of these methods.

3.1. Interference of Two Monochromatic Waves.

The electric field of the monochromatic wave may be expressed as:

$$E = A \exp\left[i\omega\left(t - \frac{z}{v}\right)\right] \tag{8}$$

One can transform this expression to obtain the product of spatially
and temporally varying factors

$$E = A \exp\left(-i\phi\right) \exp\left(i\omega t\right) \tag{9}$$

where: $\phi = \omega z/v = 2\pi n z/\lambda$ phase   n - refractive index

The product $\rho = nz$ - is the optical path between the orgin and the point z
We can than rewrite (9) as :

$$E = a \exp\left(i\omega t\right) \quad \text{where:} \quad a = A \exp\left(-i\phi\right) \tag{10}$$

Because of extremaly high frequencies of visible light waves direct
observations of the electric field are not normally possible. The only
measurable quantity is the intensity, which is the time average of the
amount of energy which, in unit time, crosses a unit area normal to the
direction of the energy flow. This is proportional to the time average
of the square of the electric field.

$$\langle E^2 \rangle = \lim_{T \to \infty} \frac{1}{2T} \int_{-T}^{T} E^2 dt = \frac{A^2}{2} \tag{11}$$

Since we are not interested in the absolute value of the intensity
but only in relative values, we can ignore this factor of 1/2, as well
as any other factors of proportionality, and define the optical intensity
as:

$$I = A^2 = |a|^2 \tag{12}$$

If two monochromatic waves propagating in the same direction and
polarized in the same plane are superposed at a point P, the total elec-
tric field at this point is:

$$E = E_1 + E_2 \tag{13}$$

where E_1 and E_2 are the electric fields due to the two wawes. If the two
waves have the same frequency, the intensity at this point is:

$$I = |A_1 + A_2|^2 \quad \text{where} \quad \begin{aligned} A_1 &= a_1 \exp(-i\phi) \\ A_2 &= a_2 \exp(-i\phi) \end{aligned} \tag{14}$$

Accordingly

$$I = A_1^2 + A_2^2 + A_1 A_2^* + A_1^* A_2 = I_1 + I_2 + 2 (I_1 I_2)^{1/2} \cos(\Delta\phi) \tag{15}$$

where I_1 and I_2 are the intensities at P due to two waves acting separa-
tely, and $\Delta\phi = \phi_1 - \phi_2$ is the phase difference between them.

If $\Delta\rho$ is the corresponding difference in the optical paths, the
order of interference is $k = \Delta\rho/\lambda$. The intensity has its maximum
value I_{max} when:

$$k = m, \quad \rho = m\lambda, \quad \Delta\phi = 2\pi m$$

where m is an integer, and its minimum value I_{min} when:

$$k = (2m + 1)/2 \quad \rho = (2m + 1)/2 \cdot \lambda \quad \Delta\phi = (2m + 1)/2 \cdot \pi$$

A convenient measure of the contrast of the interference phenomenon is
the visibility which is defined by the relation:

$$V = \frac{I_{max} - I_{min}}{I_{max} + I_{min}}$$

For two monochrometic waves polarized is the same plane with
equal amplitudes the visibility may be equal to unity.

The superimpostion of two beams may be achieved in several ways.
Fig.2 presents some of these possibilities realized in : the Michelson,
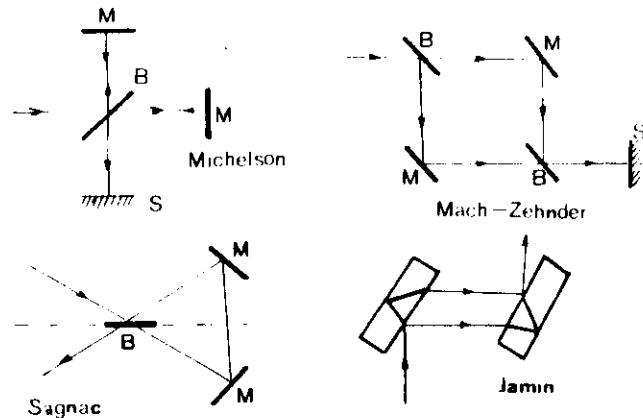Mach-Zehnder, Sagnac and Jamin interferometers.

Fig.2 Interferometer systems.

In these interferometers the two beams are obtained from a single source
by division of the amplitude over the same section of the wave front.
A surface which reflect part of the incident light and transmits part
of it is comonly used.

If in one of the arms of the interferometer a transparent object
is placed the interference fringe pattern will change according to the
changes of the optical paths caused by the object.

3.2. Some problems of interferometer designing.

In this paragraph some problems of designing of the interferometer
system will be presented, takeing as an example the arrangement used on
the PF-150 Plasma-Focus device in IPPLM.

Among a variety of possible interferometer schemes, the Mach-Zehn-
der type seems to be the most useful, as it has several advantages:

- it enables to easy separate the two beams,
- the fringus in Mach-Zehnder interferometer can be localized in
  arbitrary position,
- this kind of interferometer is manoeuvreable and versatile,
- the interferograms obtained are relativiely easy in interpre-
  tation and processing (contrary to shearing and gratting inter-
  ferometers).

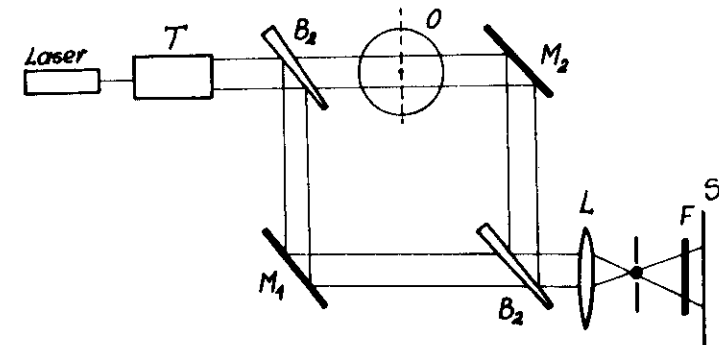The scheme of the Mach-Zehnder interferometer is presented in Fig.3.

Fig.3. The Mach-Zehnder interferometer.

The laser beam passes through the telescope (T) and its diameter
grows from initially 8 mm up to 100 mm. Then the beam is divided at the
semireflecting surface B_1 into two beams, which after reflection at the
mirrors M_1 and M_2 are recombined at the semireflecting surface B_2.
Between the beam splitter B_2 and the screen S there is a lens L placed
in such position that the symmetry plane of a plasma is at the object
plane of the lens and the screen at the image one.

In our interferometer the mirror M_2 and the beam splitter B_2 are
adjusted in such a way that two beams meet at the point O placed at the
axis of the plasma. Becouse of two wave fronts make a small angle
with each other (see fig.4) at the O plane, the interference pattern of
parallel equidistant straight lines is created on the screen in the

absence of the plasma (fig.4b). This pattern forms the reference for recording the fringe shift in the presence of the plasma.
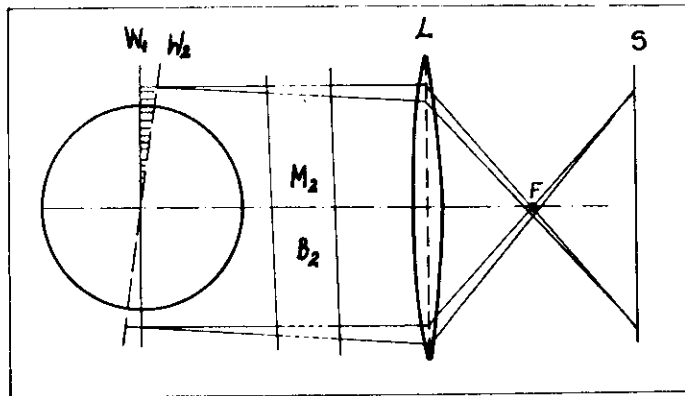

Fig.4 The geometry of wave fronts.

There are several demands the laser used in the interferometer should fulfil:

- the wave length λ of the laser should satisfy conditions (3), (5) to prevent intense absorbtion and reflection,
- the energy of the pulse should be high enough to ensure possibility of the fringes registration in the presence of the residual plasma radiation,
- the laser beam should be spatially uniform and have coherence length long enough to create good interference patterns,
- the pulse should be short enongh to prevent the fringes structure disturbance by the measured density field changes during the pulse duration.

As a source of the light for our interferometer we have chosen the rubby laser (λ = 0.694 µm) with pulse duration about 1 ns and pulse energy 100 mJ.

For the peak plasma density $2 \cdot 10^{19} \text{cm}^{-3}$ and the magnetic field below 1 MGs observed in the plasma-focus devices, relations (3), (5) are fulfiled, so the simplified formula for the refractivity index (4) may be used.

There are some limitations on the interferometer device equipped with the rubby laser used in plasma-focus phenomenon investigations. They are caused by the effect of the ray beanding on the steep density gradients. This problem will be analysed below in more detailed way. Now we can say that this kind of interferometer allowed us to investigate the plasma-focus phenomenon for initial pressure within the range 1 - 7 Torr.

The optical path difference between two arms of the interferometer caused by the presence of the plasma in one of its arms may be expressed as (Fig.5):

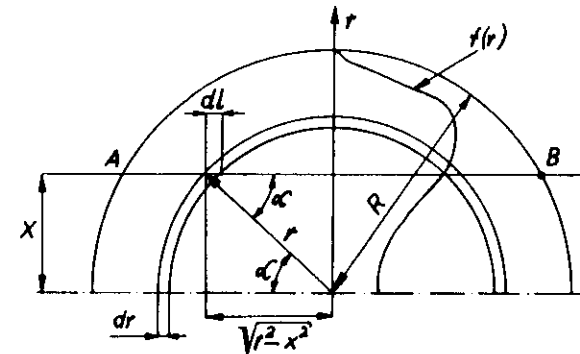$$\Delta p(x) = \int_A^B (1-n)\, dl \tag{16}$$

Fig.5. Geometry of a ray path leading to the Abel intergral.

For the axially symmetric density distribution $f(r)$ and the refractivity index:

$$n(r) \cong 1 - \frac{N_e}{2N_{cr}} = 1 - \frac{N_{emax}}{2N_{cr}} f(r) \tag{17}$$

where: N_e - electron density $[\text{cm}^{-3}]$ ($N_e = N_{e\,max} \cdot f(r)$)
N_{cr} - critical density for rubby laser $[\text{cm}^{-3}]$

one can obtain following expression for optical path difference:

$$\Delta p(x) = \frac{N_{e\,max}}{N_{cr}} \int_{x}^{R} \frac{d(r)\, r\, dr}{\sqrt{r^2 - x^2}} \qquad (18)$$

and for the phase difference:

$$\phi(x) = \frac{2\pi}{\lambda}\, \Delta p(x) \qquad (19)$$

The value of $\phi(x)$ can be determined from the interferograms obtained and than, after solving the equation (18) the density distribution can be found. The problem how to solve the equation (18) will be described in the last paragraph.

The sensitivity of the interferometer can be appreciated in the following way: for the plasma of the length L the optical path difference between two arms is equal to:

$$\Delta p = (n-1) L \qquad (20)$$

if the critical density is expressed in terms of λ ($N_{cr} = 1.12 \cdot 10^{13} \lambda^{-2}$) from (17) one can find that:

$$\Delta p = 4.46 \cdot 10^{-14} N_e \cdot L \cdot \lambda^2 \qquad N_e [cm^{-3}], L[cm], \lambda[cm] \qquad (21)$$

For the minimum detectable phase shift assumed to be $\Delta p = 0.1 \cdot \lambda$ it is possible to obtain expression for minimum plasma density measurable by the interferometer:

$$N_{e\,min} = \frac{2.24 \cdot 10^{12}}{\lambda \cdot L} \qquad (22)$$

For the rubby laser and L = 1 cm, $N_{e\,min} = 3.2 \cdot 10^{16} [cm^{-3}]$

Now, let us appreciate the capability of our interferometer arrangement to measure the plasma density in the plasma focus device. We will analise:

a) the fringes density and the resolution of the interferometer,

b) the problem of the ray deflection caused by the density gradients and demands on aperture diameters,

c) the time resolution of the interferometer for fast phenomena.

ad a) Spatial resolution of the interference fringes registration is determined by several factors:

- the abberation of optical elements used (windows of the PF chamber, lenses, mirrors etc.),

- resolution of the registering device (photographic film in our case).

It is difficulate to appreciate the total resolution of the whole optical arrangement but it is possible to determine this resolution by means of special optical tests. In this manner we have found that our interferometric system is capable to record 10 lines per milimeter.

The order of interference for the x coordinate is equal to

$$k = \Delta p / \lambda$$

Thus from (18):

$$\frac{dk}{dx} = \frac{\lambda\, N_{e\,max}}{1.12 \cdot 10^{13}} \frac{dS(x)}{dx} \quad \text{where} \quad S(x) = \int_{x}^{R} f(r)(r^2-x^2)^{1/2} r\, dr \qquad (23)$$

has a sense of the fringes density.

To check whether the fringes density connected with the presence of the plasma sheath during collapse phase of PF discharge is not greater than the resolution of the system, let us assume that the plasma density distribution has the form of parabolea characterized by two parameters: $N_{e\,max}$ and the thickness Δ (Fig.6).

With this assumption (reasonable for the outer edge of the sheath as confirmed by our measurements) the fringes density ca be found numerically from eq. (23).

Fig.7 presents results of these computations and one can see that the maximum fringes density is lower then 10 lines per milimeter for plasma density and sheath thicknesses chosen.
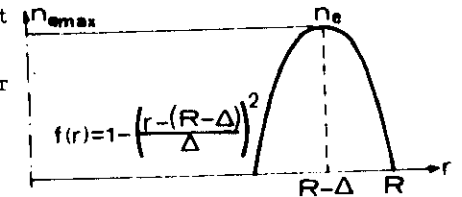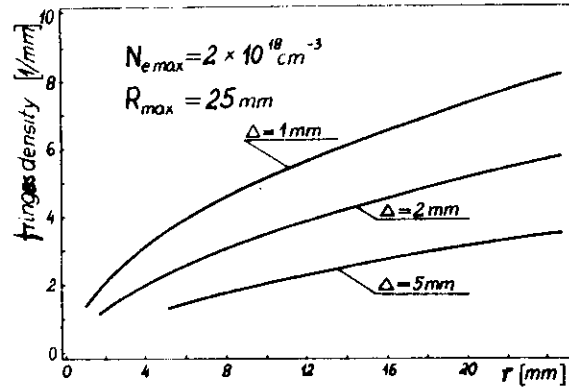

Fig.6 Assumed plasma density distribution.

Fig.7. Maximum fringe density vs. radius of the sheath.

ad b) The deflection of a ray caused by the density gradient can be
determined from the formula:

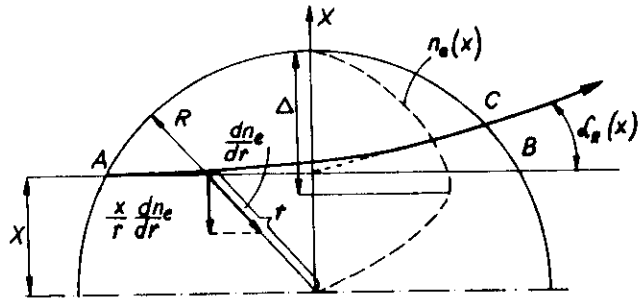$$\alpha(x) = \int_{A}^{C} \frac{1}{n} \frac{dn}{dx} \, dl \tag{24}$$

Fig.8. Ray deflection on density gradient.

If the angle α is small:

$$\alpha(x) = \frac{1}{N_{cr}} \int_{x}^{R} \frac{x}{r} \frac{dN_e}{dx} \frac{r \, dr}{\sqrt{r^2 - x^2}} \tag{25}$$

For parabolic density distribution (Fig.6) one can obtain:

$$\alpha(x) = \frac{\lambda^2 N_{e\,max}}{1.12 \cdot 10^{13}} \frac{dS(x)}{dx} \quad thus \quad \alpha(x) = \lambda \frac{dk}{dx} \tag{26}$$

It was assumed that the maksimum deflection angle record by our inter-
ferometer should be equal to α_{max} = 7 mrad.
From this assumption and relation:

$$X_{max} + S\alpha_{max} < 0.5 \, \phi_L \tag{27}$$

we have obtained diameters of optical elements (lenses, mirrors etc.).
X_{max} = inner electrode radius = 2.5 cm (PF-150 device).
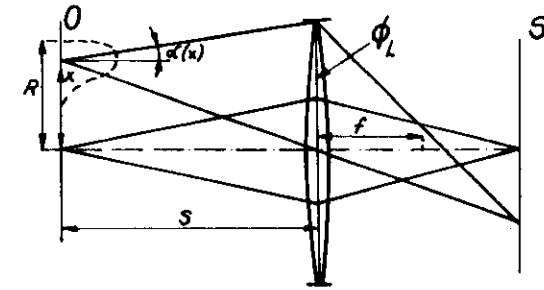S – distance from object plane to the lens (mirror).

Fig.9. Ray traces in the recording system.

ad c) Let us assume that during the exposure time τ = 1 ns the
fring pattern changes only due to displacement of the plasma
sheath as a whole with a velocity V. If the fringe shift caused
by this movement was smaller than the half distance between two
neighbouring maxima, the pattern would be legible. The following
condition should be fulfield:

$$V \cdot \tau < 0.5 \left(\frac{dk}{dx} \right)^{-1} \tag{28}$$

figure 10 illustrates the limitations of the plasma sheath density
measurement due to spatial and time resolution and ray deflection.

The sheath velocity V dependence on the radius $V(r) = 2.2 \cdot 10^7$ -
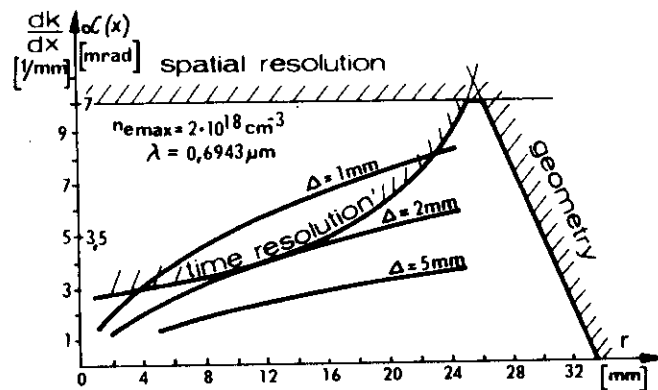- $0.7 \cdot 10^7 \cdot r$ was taken from experimental measurements.

Fig.10. The limitations of the density measurement.

The exemplary interferograms obtained with our interferometer are presented on Fig.11.

3.3. The Schieren method and shadowgraph.

The Schlieren methods are all those optical methods which record the deviations suffered by a light ray crossing a spatially nonuniform medium (the plasma in our case). If φ is the angle between the refractive gradient and the direction of the incident light, the deviation can be expressed by:

$$\alpha \cong \int_0^L \frac{1}{n} |\nabla n| \sin \varphi \, ds. \tag{29}$$

These angular displacements of the light rays can be recorded by various means, which can lead to quantitive or qualitive representation of the phenomenon. For the plasma-focus investigations, where the angle α is not very small, the quantitive methods are difficult in application. Nevertheless the Schlieren like methods may be very useful for qualitive description of the plasma dynamics. They enable to obtain
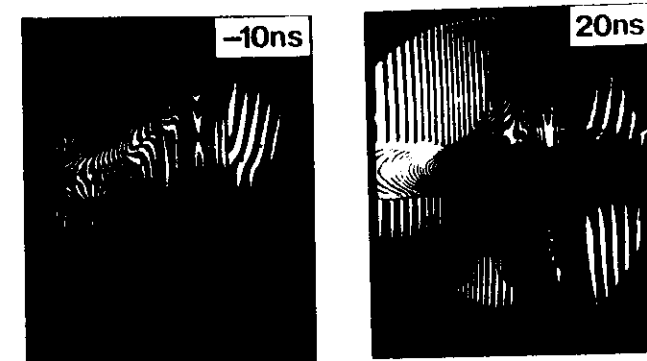

Fig.11. Interferograms of the plasma in PF device.

sharp pictures of the geometry and position of the sheath and for multiframe arrangements, the changes of this position.
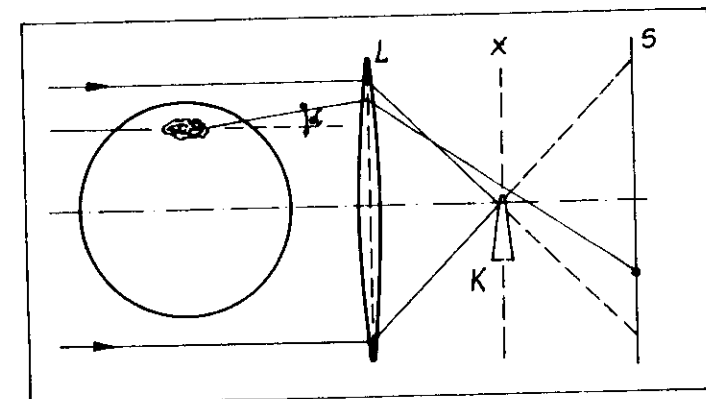

Fig.12. The Schlieren method for recording density gradients.

In the absence of the refractive index gradients the collimated laser light after passing through the lens L (fig.12) forms the bright

ring on the screen S. When the knife (named the ~~Foucaut~~ knife) is moved along X plane (focal plane of the lens), the brightness of the ring drops gradually and for some position of the knife the ring vanishes. It takes place for focus spot completly covered by the knife.

Now let us assume that in the transparent object O there is an area of the refractive index gradient. Thus the ray passing accros this area will be bended and as it is shown on Fig.12 it will pass by the knife edge creading a bright point on the screen S.

If the object is placed at the object plane of the lens and the screen S is placed in its image plane, one can obtain the picture of the refractive index gradients (density gradients) location within the object. The value of the density gradients recorded may be controlled by the position of the knife. The higher position of the knife (fig.12) the move deflected rays will reach the screen only.

The shadowgraph photography in its classic form described in literature is not very useful for PF phenomena investigations, but the change of this method which may be called an inverse Schlieren method gives the possibility to obtain a picture of the plasma sheath shape.

If in the focal plane of the lens L (Fig.13) insted of the knife the small apperture was placed, rays of the collimated laser light, deflected on the refractivity index gradients would be stopped. Thus in opposite to the Schlieren method the areas of the refractive index gradient would be black at the screen plane. When the method is used for PF investigations the shade of the plasma sheath can be recorded on the screen (Fig.13).

Fig.13. The shade of the plasma sheath in PF.

4. FARADAY ROTATION MEASUREMENTS

After traveling the length L of the magnetized plasma re(lineary polarized wave suffers a rotation of the polarization (given by:

$$\varphi = \frac{\omega\left(n_L - n_R\right)}{2c} L$$

where   is the frequency of the light and n_L, n_R, are the ref indices of the left-hand and right-hand components. By substit appropriate formulas for n_L and n_R we obtain:

$$\varphi = 2.63 \cdot 10^{-22} \lambda^2 N_e \cdot B \cdot L$$

where: λ [μm], N_e [cm^{-3}], B [kGs], L [cm]

For axially symmetric object with B_θ field the rotation be expressed by the Abel integral of the form:

$$\varphi(x) \sim \int_x^\ell \frac{N_e(r) \cdot B(r) \; r \, dr}{\sqrt{r^2 - x^2}}$$

The maximum value of φ for plasma-focus conditions ($N_{e\;max} \sim 1($ R ~ 0.2 cm, B - some hundreds kGs) is of the order of 1 - 2°, precise method for measuring small rotation angles is necessal Figure 14 shows the scheme of the diagnostic system. It consis
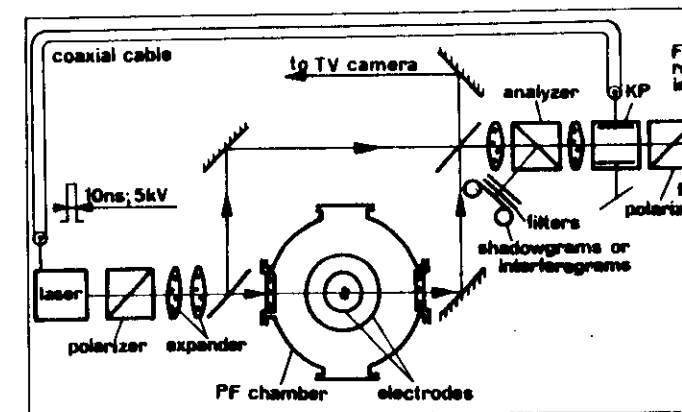

Fig.14. Experimental system for magnetic field measurements.

following subsystems:

- a pulsed ruby laser (100 mJ per 2 ns pulse),
- a system for diagnostic beam formation (Glan-Thompson polarizer
  and beam expander),
- a Mach-Zehnder interferometer,
- a polarimeter.

To analyse the FR angle the Glan-Thompson polarizer had a contrast ratio
better than 10^{-5}. Two separate diagnostic paths can be distinguished: one
for FR measurement and one for shadow picture registration, each was
equipped with an identical optical system of magnification 0.7, consis-
ting of two lenses (f_1 = 225 mm, f_2 = 158 mm). Additionally, a beam split-
ter was placed in the "shadow" path, which attenuates the light intensity
10 times to adjust it to the characteristic of photographic film used
(IZOPANCHROM-17, made in the U.S.S.R.).

The polarimeter consists of the following elements: the analyser
(Glan-Thompson), the electro-optical filter and the photographic camera.
An important element of the polarimeter is the electro-optical filter
which is composed of a Pockels cell and an additional Glan-Thompson pola-
rizer. It is used for gating of both the exposure time and the spectrum
of parasitic plasma luminescence. Filter control was achieved by applying
a voltage pulse of half-wave amplitude (for a ruby laser wavelength) of
10 ns duration to the Pockels cell. The synchronization with the diag-
nostic laser was achieved by means of a coaxial cable of suitable length.

The use of the electro-optical filter in the polarimeter increases
the signal-to-noise ratio to $E_1/E_p \cong 10^3$ (where E_1 is the laser beam
energy and E_p is the energy of parasitic luminescence of the plasma).
The polarimeter provided the registration of FR images with a spatial
resolution better than 20 lines per mm. The polarimeter-interferometer
system allowed the registration of either FR picture and shadowgraphs
or interfefograms.

The magnetic field measurement by means of the polarimeter system
described here consists of two essential steps, i.e. determination of
the FR angle and the electron density distribution. Uncertainty of the
result depends on errors connected with these two independent measure-
ments.

A FR angle is derived from the registered FR pictures and may be
read with large error. The errors are usually caused by the nonhomoge-
neous intensity distribution within the probing beam and its dumping
in plasma. In order to minimize the errors the data acquisition was do-
ne on the basis of sets of calibration curves. These were constructed
by successive exposures of the polarimeter by laser radiation of diffe-
rent intensities for the fixed turn-angle of the analyser. Thus, for
any selected angle there was a relationship between the optical density
in the Faraday channel and in the shadown channel. This is why the ab-
solute value of the FR angle in the plasma does not depend on the abso-
lute intensity of radiation entering the polarimeter. Thus the error of
FR angle readout is minimized (in our experiment its value does not exce-
ed 5 angle-minutes). Some calibration curves and the way to determine
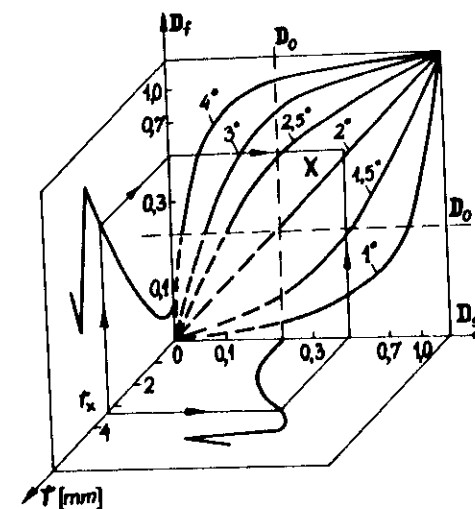the FR angle readout are shown in Fig.15.

Fig.15. The calibration curves.

Fig.16 presents a FR picture and magnetic field distribution obtained by means of the polarimeter system described. The measurements were carried out plasma-focus PF-360 device. More detailed description of the polarimeter system and results achieved using it can be found in 5).
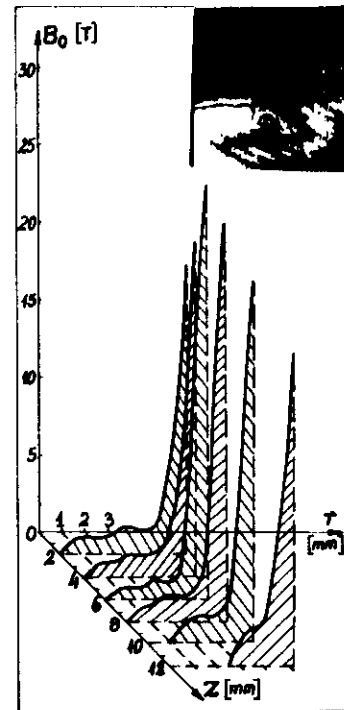

Fig.16 Magnetic field distribution in the pinch phase.

5. NUMERICAL SOLUTION TO ABEL INTEGRAL EQUATION.

The Abel integral equation:

$$y(x) = 2 \int_{x}^{1} \frac{f(r)\, r\, dr}{\sqrt{r^2 - x^2}} \quad 0 \leqslant x \leqslant 1 \quad 0 \leqslant r \leqslant 1 \tag{33}$$

permits the radial distribution (the function f(r)) to be determined by knowing, e.g. from measurements, the distribution function y(x) observed perpendiculary to the axis of the object. The physical example may be the search for the radial distribution of the refractive index of the plasma from the distribution of the interference fringes y(x).

The solution to eq (33), known under the name of the Abel integral inversion, has the form:

$$f(r) = -\frac{1}{\pi} \int_{r}^{1} \frac{y'(x)\, dx}{\sqrt{x^2 - r^2}} \tag{34}$$

or

$$f(r) = -\frac{1}{\pi r} \frac{d}{dr} \int_{r}^{1} \frac{y(x)\, x\, dx}{\sqrt{x^2 - r^2}} \tag{35}$$

The result of measurements of the function y(x) is the discrete set of the values y_k at the points x_k (k = 0,1,2 .....N). A tabulated form of the function y(x) makes it impossible to solve analytically the Abel equation, which makes the application of the numericall methods necessary.

The great variety of methods have been developed up to now for solving this equation 6).

The first step when solving numerically the Abel equation is the choice of the form of the function approximating the values y_k (in the case of the equation (34) and (35) or values f_k (in the case of of the equation (33)). Among the known methods of approximation the interpolation and the quadratic mean approximation are used, while the polynominals are employed as the approximating functions in view of their being easily integrated. After approximation of the values y_k or f_k the problem reduces to solving of the algebraic equations set. The detailed description of methods useful for the Abel equation solving can be found e.g. in 6).

We would like to point out to two problems: testing of the methods and sensitivity of methods to measuring errors.

It is necessary to test the numerical methods to be used for solving Abel equation. The known analyticall solutions of the Abel equation presented on Fig.6 may be useful in this aim.

In order to illustrate the effect of the measuring errors upon the quality of the reproduction of the function f(r) by different methods of the Abel equation solving, the calculations have been performed for the first test function (Fig.16), with a superimposed "noise". The results of the calculation are reproduced in Fig.17.

One can see that there is a great difference of this quality and careful testing of the method is necessary before utilisation.

The methods making use of the least-squares approximation give better results in this situation.
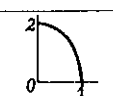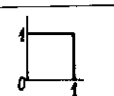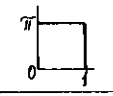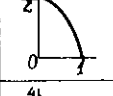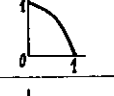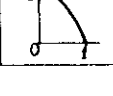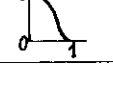
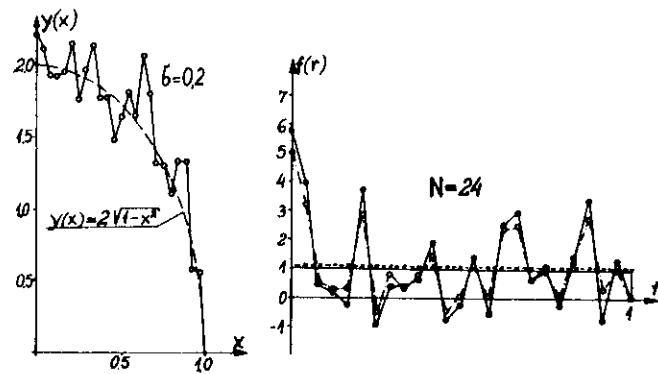| $y(x)$	$f(r)$
$y(x)=2\sqrt{1-x^2}$	$f(r)=1$
$y(x)=\pi$	$f(r)=\dfrac{1}{\sqrt{1-x^2}}$
$y(x)=\dfrac{\pi}{2}(1-x^2)$	$f(r)=\sqrt{1-r^2}$
$y(x)=\dfrac{4}{3}\sqrt{(1-x^2)^3}$	$f(r)=1-r^2$

Fig.16 Formulas and graphs of test functions.

Fig.17 Effect of measuring errors upon reproduction quality of function f(r).

REFERENCES

1) Jolas, A., Rapport CEA-R-5153

2) Bernard, J.E., et al, Phys.Fluids, 30, 11, 3616-3623, 1987

3) Martellucci, S., Suppl.Nuovo Cimento V, No 3, 642-679, (1967).

4) Jahoda, F.C. and Sawyer, G.A., in Methods of Experimental Physics Vol.9B (Academic Press, New York, 1971), Chap.II.

5) Czekaj,S., et al., Plasma Physics and Controlled Fusion, 31, No.4, 587-594, (1989).

6) Kasperczuk, A., et al., Journal Technical Physics, 19, No.1, 137-150, (1978).